

Pre-training Everywhere: Parameter-Efficient Fine-Tuning for Medical Image Analysis via Target Parameter Pre-training

Xingliang Lei^{1†}, Yiwen Ye^{1†}, Ziyang Chen¹, Minglei Shu², Yong Xia^{1, 3, 4✉}

¹National Engineering Laboratory for Integrated Aero-Space-Ground-Ocean Big Data Application Technology, School of Computer Science and Engineering, Northwestern Polytechnical University, China

²Shandong Artificial Intelligence Institute, Qilu University of Technology (Shandong Academy of Sciences), China

³Ningbo Institute of Northwestern Polytechnical University, Ningbo 315048, China

⁴Research & Development Institute of Northwestern Polytechnical University in Shenzhen, Shenzhen 518057, China
{leixingliang, ywye, zychen}@mail.nwpu.edu.cn, shuml@sdas.org, yxia@nwpu.edu.cn

Abstract

Parameter-efficient fine-tuning (PEFT) techniques have emerged to address issues of overfitting and high computational costs associated with fully fine-tuning in the paradigm of self-supervised learning. Mainstream methods based on PEFT involve adding a few trainable parameters while keeping the pre-trained parameters of the backbone fixed. These methods achieve comparative, and often superior, performance to fully fine-tuning, demonstrating the powerful representation ability of the pre-trained backbone. Despite its success, these methods typically ignore the initialization of the new parameters, often relying solely on random initialization. We argue that if pre-training is significantly beneficial, it should be applied to all parameters requiring representational capacity. Motivated by this insight, we propose a simple yet effective fine-tuning framework based on Target Parameter Pre-training (TPP). The target parameters refer to the new parameters introduced during fine-tuning. TPP includes an additional stage before PEFT to pre-train these target parameters. During this stage, the pre-trained backbone parameters are frozen, and only the target parameters are trainable. A defined pre-text task is used to encourage the target parameters to learn specific representations of downstream data. When PEFT is subsequently employed, the pre-trained target parameters are loaded to enhance fine-tuning efficiency. The proposed TPP framework is versatile, allowing for the integration of various pretext tasks for pre-training and supporting different PEFT methods as backbones. We evaluated the fine-tuning performance of our method using five public datasets, including three modalities and two task types. The results demonstrate that the proposed TPP can be easily integrated into existing PEFT methods, significantly improving performance.

Introduction

Deep learning has significantly advanced medical image analysis, markedly improving model performance (Ronneberger, Fischer, and Brox 2015; Zhou et al. 2019). However, these models often require large-scale, high-quality annotated datasets, which are particularly time-consuming

[†]X. Lei and Y. Ye contributed equally to this work. Corresponding author: Y. Xia.

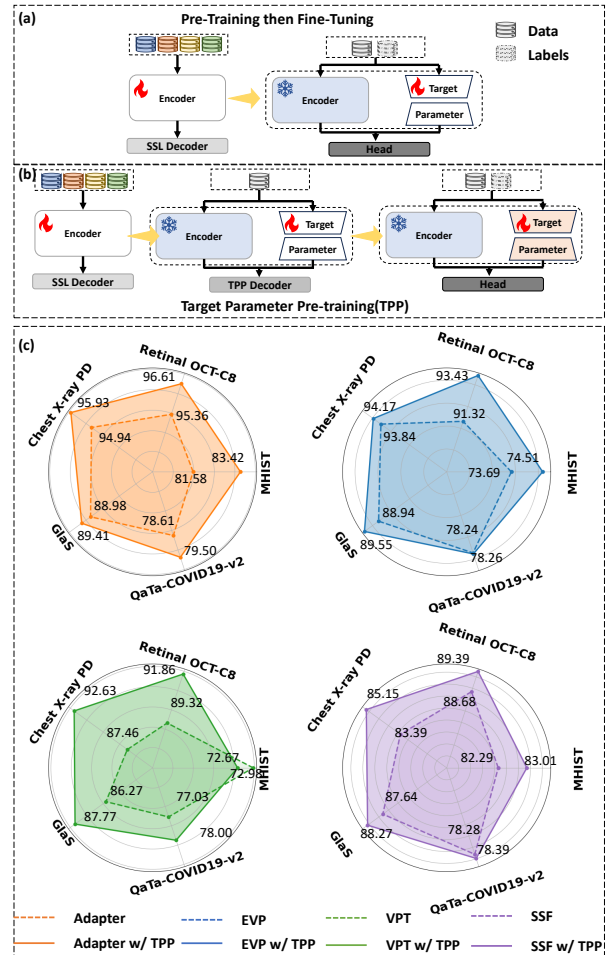


Figure 1: Comparison between (a) traditional pre-training paradigm, *i.e.*, pre-training then fine-tuning, and (b) our TPP framework. The newly introduced stage is inserted between the pre-training stage and fine-tuning stage and is used to pre-train the target parameters. (c) Performance comparison of PEFT methods and PEFT methods with TPP, represented by using dashed and solid lines, respectively. The different colors represent different PEFT methods.

and labor-intensive to produce in the field of medical imaging (Dutt et al. 2023a). Consequently, medical image analysis often faces challenges related to limited dataset sizes (Willeminck et al. 2020), which hinders its clinical application.

Self-supervised learning (SSL) has gained prominence due to its reduced data requirements, high accuracy, and strong generalization capabilities. SSL typically involves two stages: pre-training on a large-scale unlabeled dataset and fine-tuning on labeled datasets. While diverse pretext tasks are used for pre-training, SSL methods (Chen et al. 2020; Azizi et al. 2021) generally update all pre-trained parameters during fine-tuning. This approach can be problematic for medical imaging tasks with limited fine-tuning datasets, as updating all pre-trained parameters on a small dataset can compromise model robustness and increase the risk of overfitting. Additionally, it incurs high computational and storage costs due to the need to update and store all model parameters for each downstream task.

To address these challenges, parameter-efficient fine-tuning (PEFT) has emerged as a promising solution (Dutt et al. 2023b). PEFT typically involves freezing pre-trained parameters and either updating a subset of these parameters (Zaken, Ravfogel, and Goldberg 2021; Touvron et al. 2022) or adding a small set of new trainable parameters, known as *target parameters* (Hu et al. 2021; Houlsby et al. 2019; Chen et al. 2022; Fu, Zhu, and Wu 2024; Sung, Cho, and Bansal 2022; Jia et al. 2022; Li and Liang 2021; Wang et al. 2024; He et al. 2023), as shown in Figure 1(a). Methods that add target parameters have demonstrated superior performance and utilize only a small number of new parameters. However, although these methods leverage the robust representations of pre-trained models, they do not fully exploit the advantages of pre-training. We argue that *if the backbone is pre-trained, the newly added parameters should also be pre-trained*.

In this paper, we propose a straightforward yet effective fine-tuning framework based on Target Parameter Pre-training (TPP). Our TPP framework focuses on the new parameters introduced by PEFT methods, excluding task-specific heads (*i.e.*, linear layers for classification or decoders for segmentation), which we refer to as target parameters. Unlike existing PEFT strategies that directly fine-tune pre-trained models with randomly initialized target parameters, our approach introduces a target parameter pre-training stage between pre-training and fine-tuning, as shown in Figure 1(b). This stage involves pre-training the target parameters by freezing the well-pre-trained backbone and updating only the target parameters through a pretext task. Specifically, we pre-train the target parameters for each downstream dataset using its training data, enabling them to learn dataset-specific representations. We evaluated our TPP framework against several existing efficient fine-tuning methods using five public datasets. Our TPP framework is a plug-and-play solution compatible with any PEFT method that adds target parameters, consistently improving the fine-tuning performance of these methods, as shown in Figure 1(c).

The contributions of this work are three-fold.

- We propose a plug-and-play PEFT framework called TPP for medical image classification and segmentation tasks. This framework can be easily integrated into existing PEFT methods based on adding target parameters without requiring modifications.
- Building on the insight that if the backbone is pre-trained, the target parameters should also be pre-trained, we propose a target parameter pre-training stage that optimizes target parameters for specific downstream data.
- The TPP framework consistently enhances PEFT baselines across five datasets, including both classification and segmentation tasks.

Related Work

Parameter-efficient Fine-tuning

PEFT techniques effectively minimize the need for updating all model parameters by requiring adjustments to only a select few. An intuitive solution is to update specific parameters of the pre-trained model, such as biases (Zaken, Ravfogel, and Goldberg 2021), layer normalization (Basu et al. 2024), batch normalization (Frankle, Schwab, and Morcos 2020), and attention mechanisms (Touvron et al. 2022). However, this approach often disrupts the knowledge encoded in the pre-trained model, leading to suboptimal fine-tuning performance.

To address this issue, recent research has focused on introducing new trainable parameters, referred to as target parameters. In this strategy, the parameters of the pre-trained backbone are kept fixed while the target parameters are updated using downstream datasets. This strategy can be categorized into four main categories. (1) Adapter (Houlsby et al. 2019): This method inserts parallel or serial blocks to output residuals. For example, Adapter (Houlsby et al. 2019) inserts a bottleneck block with residual connections serially between the feed-forward layer of Transformer blocks. Adapterformer (Chen et al. 2022) uses a similar bottleneck deconstruction without residual connections in parallel within the MLP section of Transformer blocks. (2) Low-Rank Adaptation (LoRA) (Hu et al. 2021): This approach introduces learnable low-rank matrices into the self-attention layers of Transformers. LoRA is highly parameter-efficient and integrates seamlessly with the pre-trained backbone during inference, minimizing additional computational overhead. Variants like ConvLoRA (Zhong et al. 2024) and AdaLoRA (Zhang et al. 2023) further enhance LoRA by incorporating lightweight convolutional parameters or adaptively allocating parameter budgets based on importance scores. (3) Prompting: This method modifies the input to Transformer layers by adding learnable tokens. For example, VPT (Jia et al. 2022) and its variants (He et al. 2023; Yoo et al. 2023) introduce learnable tokens to the inputs of Transformer layers for visual tasks. (4) Side-tuning (Huang et al. 2024; Fu, Zhu, and Wu 2024; Yin et al. 2023; Tang et al. 2024): This technique involves using a side model that operates independently of the frozen backbone, thus avoiding gradient back-propagation through the backbone. For instance, DTL (Fu, Zhu, and Wu 2024) employs a lightweight Compact Side Network (CSN) to capture task-specific features through

low-rank linear mappings, which are then integrated back into the backbone.

Despite achieving promising results, many existing methods initialize target parameters randomly (e.g., zero, uniform, or normal distributions) (Houlsby et al. 2019; Hu et al. 2021; Lian et al. 2022; Jia et al. 2022). For instance, Adapter blocks are often initialized to approximate the identity function with zero initialization, while LoRA’s two low-rank matrices are typically initialized to zero and random respectively. These methods aim to ensure that target parameters do not alter the input to the original layer initially (Liao, Tan, and Monz 2024). However, this approach overlooks the potential benefits of pre-training, which could provide high-quality, task-specific representations.

Recent efforts have sought to address this gap by improving target parameter initialization. Self-Prompt Tuning (Wang et al. 2024) uses token prototypes derived from target data as initial prompts. PVP (Song et al. 2023) pre-trains target parameters on a large-scale dataset, and Su *et al.* (Su et al. 2021) initializes target parameters with soft prompts pre-trained on related tasks. Nonetheless, these methods do not address the issue of selecting appropriate datasets for pre-training target parameters. We argue that if pre-training on downstream data is necessary, it should be leveraged directly. Thus, the proposed TPP aims to enhance the initialization of target parameters by pre-training them specifically for the target dataset, thereby improving efficient fine-tuning.

Self-supervised Learning Methods

Self-supervised Learning (SSL) is an advanced technique for representation learning (Chen et al. 2020; He et al. 2020; Caron et al. 2021; Michelucci 2022; Vincent et al. 2008; He et al. 2022). SSL typically involves two stages: unsupervised pre-training with a pretext task and supervised fine-tuning on target data.

Various pretext tasks have been explored, including contrastive learning (Chen et al. 2020; He et al. 2020; Caron et al. 2021), generative learning (Michelucci 2022; Vincent et al. 2008; He et al. 2022), and their combinations (Goodfellow et al. 2020). For instance, MAE (He et al. 2022) employs masked image modeling, where an image is divided into patches, most of which are randomly masked. The model learns to predict these masked patches from the remaining visible ones. DINO (Caron et al. 2021) combines multi-crop learning (Caron et al. 2020) with self-distillation for contrastive learning, using centering and sharpening operations to prevent collapse in the momentum teacher model’s output vectors. After SSL pre-training, the model can provide high-quality representations, which reduces reliance on large annotated datasets and accelerates convergence. This capability is valuable for various tasks, including classification (Zhou et al. 2021; Ye et al. 2024), localization (Yang et al. 2021; Siméoni et al. 2021), and segmentation (Zhou et al. 2021; Ye et al. 2024; Gharawi, Alahmadi, and Ramaswamy 2023; Ye et al. 2022).

Despite the benefits of SSL, parameter-efficient fine-tuning (PEFT) methods often initialize new parameters randomly, which undermines the advantages of pre-training. To

address this, our study introduces an additional stage for pre-training these new parameters before fine-tuning, thereby leveraging the full potential of SSL.

Method

Preliminaries

Paradigm of SSL. SSL typically involves two stages: pre-training and fine-tuning. Let D_{un} denote a large-scale unlabeled dataset, and θ represent the parameters of the backbone network. In the pre-training stage, θ is trained on D_{un} by completing a pretext task, which does not require human-labeled data for supervision. The parameters obtained after pre-training, denoted as θ^p , exhibit strong transferability to various downstream tasks. In the fine-tuning stage, a labeled dataset D_l is used to adapt the pre-trained backbone to the target task. This is achieved by adding a new task-specific head, represented by θ_{head} , and updating all parameters. The process of a single feed-forward operation can be described as:

$$P = f(I, \langle \theta^p, \theta_{head} \rangle), I \in D_l, \quad (1)$$

where I is the input image, $\langle \cdot \rangle$ denotes the set of parameters involved in the feed-forward process $f(\cdot)$, and P is the output.

Pre-trained Backbone. For this study, we employ MedCoSS (Ye et al. 2024) as the pre-trained backbone, due to its large-scale multi-modal pre-training and robust generalization ability across downstream tasks with various modalities. MedCoSS is based on ViT/B (Dosovitskiy et al. 2020) and is pre-trained using the pretext task of masked modeling (Devlin et al. 2018; He et al. 2022).

PEFT based on adding new parameters. Leveraging the enhanced representation capabilities of pre-trained models, promising results can be achieved by freezing the pre-trained model parameters and introducing new, trainable parameters, termed target parameters θ_{tp} . The feed-forward process can then be described as:

$$P = f(I, \langle \|\theta^p\|, \theta_{tp}, \theta_{head} \rangle), I \in D_l, \quad (2)$$

where $\|\cdot\|$ indicates the frozen parameters.

Target Parameter Pre-training

To address the limitations of randomly initialized target parameters, which do not fully exploit the benefits of pre-training, we introduce a TPP stage, which occurs between the self-supervised pre-training and the fine-tuning phases. During TPP, we freeze the pre-trained backbone parameters, denoted as θ^p , while keeping the target parameters θ_{tp} trainable. Using a target dataset D_l , we pre-train θ_{tp} by performing a pretext task. The specific pre-training process varies depending on the choice of pretext task. In our experiments, we explored two pretext tasks: MAE (He et al. 2022) and DINO (Caron et al. 2021), to validate the generalization ability of TPP.

TTP based on MAE. MAE is a generative SSL method that enhances image reconstruction by appending a transformer-based decoder to the backbone. This method partitions an image into multiple patches, randomly masks 75% of them, and uses the visible patches to predict the masked ones. The

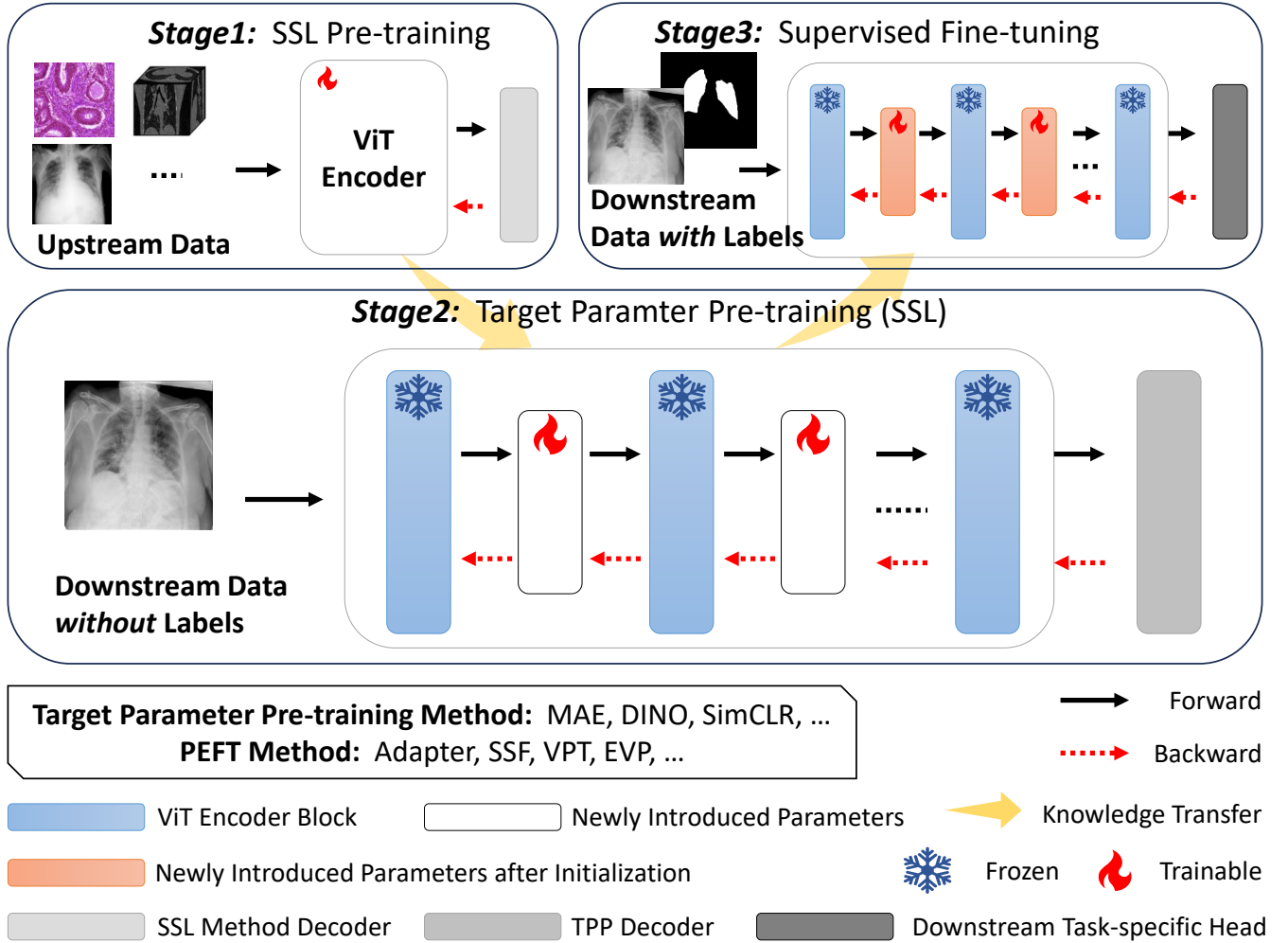


Figure 2: Overview of the proposed TPP framework. It introduces a pre-training stage for target parameters between the traditional self-supervised learning pre-training and the subsequent supervised fine-tuning stages.

model is trained using a mean squared error (MSE) loss function to minimize the reconstruction error.

TTP based on DINO. DINO employs contrastive learning in self-supervised settings by appending a multi-layer perceptron (MLP) to the backbone, forming a student model that maps the backbone’s output features to a high-dimensional latent space. A momentum-based variant of this student model, called the teacher model, provides supervision. For each image, strong data augmentations generate two distinct views, which are processed by both the student and teacher models. The student model is trained to maximize the similarity of the output vectors to those of the teacher model using a cross-entropy loss function.

Using these SSL methods, we obtain the pre-trained target parameters θ_{tp}^p . These parameters, along with θ^p , are then transferred to the target dataset D_l . Following PEFT methods, we freeze θ^p and keep θ_{tp}^p and θ_{head} trainable. The forward pass is defined as:

$$P = f(I, \langle |\theta^p|, \theta_{tp}^p, \theta_{head} \rangle), I \in D_l. \quad (3)$$

Dataset	Modality	Task	Train	Val	Test
MHIST	Path.	Cls	3152	-	-
Chest X-ray PD	X-ray	cls	4575	-	-
Retinal OCT-C8	OCT	Cls	18400	2800	2800
GlaS	Path.	Seg	85	-	80
QaTa	X-ray	Seg	7145	-	2113

Table 1: Overview of the datasets used in this study.

Our TPP framework is designed to be a plug-and-play solution, seamlessly integrating with any PEFT method that utilizes target parameters without requiring modifications.

Experiments

Datasets

In this study, we evaluated our TPP framework using five downstream datasets: the MHIST dataset, the Retinal OCT-C8 dataset, the Chest X-ray PD dataset, the GlaS dataset, and the QaTa-COVID19-v2 (QaTa) dataset. A summary of

Method	MHIST				Retinal OCT-C8				Chest X-ray PD			
	ACC	AUC	F1	Ratio	ACC	AUC	F1	Ratio	ACC	AUC	F1	Ratio
Full Fine-tuning	83.11	89.78	81.60	100.0	94.54	99.64	94.53	100.0	96.04	99.41	96.02	100.0
Linear Probe	68.99	77.08	66.46	0.003	59.96	92.64	59.42	0.008	69.86	96.56	60.55	0.004
EVP	73.69	81.34	71.82	0.961	91.32	99.34	91.31	0.966	93.84	99.03	93.77	0.962
VPT	72.98	79.84	71.35	0.103	89.32	99.04	89.25	0.108	87.46	96.62	87.30	0.103
SSF	82.29	89.29	80.85	0.172	88.68	98.93	88.66	0.177	83.39	98.18	81.76	0.173
BitFit	82.40	89.60	80.86	0.115	87.18	98.81	87.13	0.120	83.50	97.73	82.14	0.116
Adapter	81.58	89.09	80.16	3.045	95.36	99.74	95.36	3.050	94.94	99.45	94.89	3.046
Adaptformer	66.02	74.30	65.07	3.831	82.32	98.11	82.37	3.836	75.47	91.35	74.43	3.832
DTL	77.48	84.85	75.09	0.051	89.79	99.13	89.81	0.055	89.55	97.99	89.17	0.051
Adapter w/ TPP	83.42	91.38	82.21	3.045	96.61	99.77	96.61	3.050	95.93	99.21	95.91	3.046

Table 2: Results of Adapter with TPP, full fine-tuning, and eight PEFT methods on three classification downstream tasks. The best result on each column is highlighted in **bold**. Ratio denotes the ratio of target parameters to total parameters.

Method	GlaS			QaTa		
	Dice	HD	Ratio	Dice	HD	Ratio
Full Fine-tuning	88.84	47.41	100.0	78.63	29.54	100.0
Linear Probe	86.56	61.85	2.000	73.62	39.46	2.000
EVP	88.94	49.10	2.940	78.24	31.67	2.940
VPT	86.27	52.23	2.100	77.03	33.43	2.100
SSF	87.64	54.49	2.170	78.28	30.53	2.170
BitFit	87.56	58.58	2.110	77.99	32.30	2.110
Adapter	88.98	49.06	4.980	78.61	29.91	4.980
Adaptformer	86.62	61.43	5.750	74.97	36.23	5.750
DTL	87.52	55.11	2.047	73.99	38.29	2.047
Adapter w/ TPP	89.41	44.25	4.980	79.50	29.28	4.980

Table 3: Results of Adapter with TPP, full fine-tuning, and eight PEFT methods on two segmentation downstream tasks. The best result on each column is highlighted in **bold**. Ratio denotes the ratio of target parameters to total parameters.

these datasets is provided in Table 1. Specifically, **MHIST dataset (Wei et al. 2021)**. This dataset contains 3,152 colorectal polyp images, each labeled as either hyperplastic polyps (HP) or sessile serrated adenomas (SSA). Due to the absence of official splits, we randomly divided the data into 70% for training, 10% for validation, and 10% for testing. **Retinal OCT-C8 dataset (Subramanian et al. 2022)**. This dataset includes 24,000 OCT 2D images categorized into eight groups: age-related macular degeneration (AMD), choroidal neovascularization (CNV), central serous retinopathy (CSR), diabetic macular edema (DME), macular hole (MH), choroidal drusen (DRUSEN), diabetic retinopathy (DR), and normal retina (NORMAL). We adhered to the official data split for training, validation, and test sets. **Chest X-ray PD dataset (Asraf and Islam 2021)**. This dataset includes 4,575 2D chest X-ray images, categorized into COVID-19 infections, other pneumonia infections, and healthy individuals. We applied a data split strategy similar to that used for the MHIST dataset. **GlaS dataset (Sirinukunwattana et al. 2017)**. This dataset contains 165 pathological images of H&E-stained colon tissue sections, labeled as malignant or benign. **QaTa-COV19v2(QaTa) dataset (Degerli et al. 2022)**. This dataset is used for segmenting COVID-19 infected regions. It consists of 7,145

training images and 2,113 test images. For the GlaS and QaTa datasets, we followed the official data splits and randomly selected 20% of the training data from each category as the validation set.

Implementation Details

For target parameter pre-training using MAE, we followed the approach outlined in previous studies (Ye et al. 2024; He et al. 2022). We employed the AdamW optimizer (Loshchilov, Hutter et al. 2017), initializing the learning rate at $1.5e-3$ with a weight decay of $1.5e-2$, and used a batch size of 64. The pre-training was conducted for a maximum of 500 epochs for classification tasks and 1000 epochs for segmentation tasks, the latter necessitating more epochs due to the smaller sample sizes in segmentation datasets. A warm-up strategy was implemented over the first 40 epochs, gradually increasing the learning rate from 0 to $1.5e-3$, followed by a cosine decay to zero during the remainder of the training.

For the target parameter pre-training using DINO, we adhered to the method described in (Caron et al. 2021). The AdamW optimizer was utilized with a batch size of 64. The learning rate was linearly warmed up over the initial 10 epochs, increasing to a base value determined by the linear scaling rule: $lr=0.0001 \times \text{batch size}/256$. Post-warmup, the learning rate was decayed according to a cosine schedule. Similarly, weight decay was adjusted using a cosine schedule, ranging from 0.04 to 0.4. We applied data augmentations similar to those used in BYOL, including color jittering, Gaussian blur, and solarization.

During the fine-tuning stage, we adhered to the fine-tuning framework outlined by MedCoSS (Ye et al. 2024). The target parameters, initially obtained from the TTP using MAE, were employed as the default configuration. We utilized the AdamW optimizer (Loshchilov, Hutter et al. 2017), with hyperparameters customized to suit the specific downstream tasks. Further details can be found in the Appendix.

Evaluation Metrics

For classification tasks, we employed the area under the receiver operator curve (AUC, %), accuracy (ACC, %), and F1 score (F1, %) as metrics. Performance in segmentation tasks

Method	MHIST			Retinal OCT-C8			Chest X-ray PD			GlaS		QaTa	
	ACC	AUC	F1	ACC	AUC	F1	ACC	AUC	F1	Dice	HD	Dice	HD
Adapter	81.58	89.09	80.16	95.36	99.74	95.36	94.94	99.45	94.89	88.98	49.06	78.61	29.91
Adapter w/ TPP	83.42	91.38	82.21	96.61	99.77	96.61	95.93	99.21	95.91	89.41	44.25	79.50	29.28
EVP	73.69	81.34	71.82	91.32	99.34	91.31	93.84	99.03	93.77	88.94	49.10	78.24	31.67
EVP w/ TPP	74.51	82.17	72.13	93.43	99.47	93.43	94.17	99.14	94.13	89.55	48.06	78.26	31.23
VPT	72.98	79.84	71.35	89.32	99.04	89.25	87.46	96.62	87.30	86.27	52.23	77.03	33.43
VPT w/ TPP	72.67	80.19	71.55	91.86	99.28	91.85	92.63	98.62	92.55	87.77	57.06	78.00	31.98
SSF	82.29	89.29	80.85	88.68	98.93	88.66	83.39	98.18	81.76	87.64	54.49	78.28	30.53
SSF w/ TPP	83.01	90.50	81.72	89.39	99.05	89.35	85.15	97.38	84.11	88.27	57.36	78.39	31.09

Table 4: Results on four PEFT Methods based on TPP. For TPP, we used MAE as the pretext task. We highlight in **bold** the better results comparing each PEFT method with and without TPP.

	MHIST			QaTa	
	ACC	AUC	F1	Dice	HD
Adapter	81.58	89.09	80.16	78.64	30.54
Adapter w/ TPP	82.29	88.59	81.29	79.11	29.27
VPT	72.98	79.84	71.35	77.03	33.43
VPT w/ TPP	74.31	81.21	71.97	77.06	32.81
SSF	82.29	89.29	80.85	78.28	30.53
SSF w/ TPP	83.32	90.69	82.04	78.61	30.97

Table 5: Results on three PEFT methods based on TPP. For TPP, we used DINO as the pretext task. We highlight in **bold** the better results comparing each PEFT method with and without TPP.

was evaluated based on the Dice similarity coefficient (Dice, %) and the 95% Hausdorff distance (HD).

Comparisons with state-of-the-art Methods

We compared our TPP with eight PEFT methods, including Linear Probe, EVP (Liu et al. 2023), VPT (Jia et al. 2022), SSF (Lian et al. 2022), BitFit (Zaken, Ravfogel, and Goldberg 2021), Adapter (Houlsby et al. 2019), AdapterFormer (Chen et al. 2022), and DTL (Fu, Zhu, and Wu 2024), on the MHIST, Retinal OCT-C8, Chest X-ray PD, GlaS, and QaTa datasets. Full fine-tuning involves updating all model parameters, whereas Linear Probe only updates the task-specific head. The results shown in Tables 2 and 3 reveal that (1) among the PEFT methods, Adapter achieves the best generalization performance across all datasets; (2) applying the proposed TPP to Adapter results in significant performance improvements on all datasets. For instance, TPP enhances Adapter’s performance on the MHIST dataset by 1.84%, 2.29%, and 2.05% in terms of ACC, AUC, and F1, respectively. Additionally, TPP introduces improvements of 0.43% in Dice and 4.81 in HD on the GlaS dataset; and (3) compared to full fine-tuning, Adapter with TPP outperforms it on the MHIST, Retinal OCT-C8, GlaS, and QaTa datasets while updating only approximately 3%, 3%, 5%, and 5% of the parameters, respectively. However, for the Chest X-ray PD dataset, our method performs slightly below full fine-tuning.

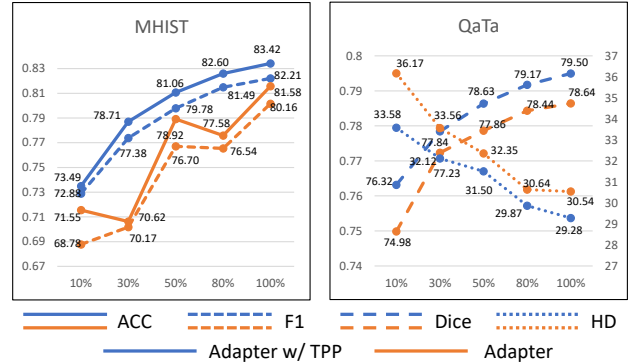


Figure 3: Results of Adapter with and without TPP on the MHIST and QaTa with 10%, 30%, 50%, 80%, and 100% training data.

Other PEFT Methods with TPP

In the previous section, we demonstrated the substantial improvement of our TPP method over the Adapter. To further validate its effectiveness, we extended our experiments to include three additional PEFT methods: EVP, VPT, and SSF. We conducted experiments on these PEFT methods with and without TPP. The results, presented in Table 4, confirm the robustness of our TPP approach, showing consistent positive effects across most metrics and datasets. For instance, the combination of EVP with TPP surpasses the performance of EVP alone across all datasets, including both classification and segmentation tasks. Specifically, on the MHIST dataset, EVP combined with TPP yields performance improvements of 0.82%, 0.83%, and 0.31% in terms of ACC, AUC, and F1 scores, respectively, compared to EVP alone. Similarly, on the GlaS dataset, the addition of TPP to EVP results in gains of 0.61% in Dice and 1.04 in HD over EVP.

TPP based on DINO

The default pre-training pretext task is MAE. In this section, we employed DINO (Caron et al. 2021) as the pretext task and evaluated three PEFT methods: Adapter, VPT, and SSF, as summarized in Table 5. The results demonstrate that our TPP approach, when using DINO, can also enhance fine-tuning performance, achieving superior results across nearly all metrics. Take Adapter as an example, Adapter with TPP

	MHIST			Retinal OCT-C8			Chest X-ray PD			GlaS		QaTa	
	ACC	AUC	F1	ACC	AUC	F1	ACC	AUC	F1	Dice	HD	Dice	HD
Zero	81.58	89.09	80.16	95.36	99.74	95.36	94.94	99.45	94.89	88.98	49.06	78.61	29.91
Transfer	82.91	89.51	81.38	94.61	99.66	94.62	95.49	99.49	95.45	89.46	42.85	79.13	29.93
TPP w/ DINO	82.29	88.59	81.29	96.25	99.75	96.24	95.71	99.56	95.67	88.60	46.98	79.11	29.27
TPP w/ MAE	83.42	91.38	82.21	96.61	99.77	96.61	95.93	99.21	95.91	89.41	44.25	79.50	29.28

Table 6: Results on different initialization strategies. We used Adapter as the baseline. Zero means initializing adapter blocks to approximate an identity function through zero initialization. Transfer means initializing target parameters by pre-training on a larger, similar dataset. The best result on each column is highlighted in **bold**.

	Modality	MHIST			GlaS		Chest X-ray PD			QaTa		Retinal OCT-C8		
		ACC	AUC	F1	Dice	HD	ACC	AUC	F1	Dice	HD	ACC	AUC	F1
MHIST	Path.	83.42	91.38	82.21	89.65	45.54	95.16	99.38	95.11	78.84	29.69	96.00	99.74	95.99
GlaS		82.40	89.56	81.25	89.41	44.25	95.27	99.39	95.22	78.99	29.72	96.07	99.74	96.07
Chest X-ray PD	X-ray	79.12	88.16	78.04	88.51	50.36	95.93	99.21	95.91	78.76	30.13	95.71	99.78	95.72
QaTa		79.63	87.96	78.30	89.20	44.27	95.05	99.54	95.00	79.50	29.28	95.89	99.74	95.88
Retinal OCT-C8	OCT	81.78	89.32	80.06	88.32	47.75	94.83	99.29	94.76	78.68	30.23	96.61	99.77	96.61
Adapter	-	81.58	89.09	80.16	88.98	49.06	94.94	99.45	94.89	78.61	29.91	95.36	99.74	95.36

Table 7: Results of Adapter and different TPP variants with pre-training on one dataset and fine-tuning on another dataset. The pretext task is MAE and the fine-tuning framework is Adapter. The best result on each column is highlighted in **bold**.

achieves 0.71%, 1.13%, 0.47%, 1.27 improvements in terms of MHIST’s ACC, MHIST’s F1, QaTa’s Dice, and QaTa’s HD, respectively. For the AUC of MHIST, Adapter is 0.5% higher than the one with TPP.

Fine-tuning with Fewer Annotations

We evaluated the performance of the Adapter, both with and without TPP, on the MHIST and QaTa datasets by progressively increasing the ratios of training annotations from 10% to 100%, as depicted in Figure 3. As the number of training data increases, the performance of the model tends to improve. Throughout this process, Adapter with TPP consistently outperforms the Adapter on both the classification dataset MHIST and the segmentation dataset QaTa, demonstrating the effectiveness of TPP across different training annotations.

Initialization of Target Parameters

We experimented with various initialization strategies, including Zero, Transfer, TPP with DINO, and TPP with MAE. The Zero initialization strategy (Houlsby et al. 2019) initializes adapter blocks to approximate an identity function through zero initialization. The Transfer strategy initializes target parameters by pre-training on a larger, similar dataset, as described in (Su et al. 2021; Song et al. 2023). For implementation, we utilized CRAG (Awan et al. 2017), OCT2017 (Kermany et al. 2018), NCH (Kather, Halama, and Marx 2018), MHIST (Wei et al. 2021), and ChestXR (Akhloufi and Chetoui 2021) as similar datasets for MHIST, Retinal OCT-C8, Chest X-ray PD, GlaS, and QaTa, respectively. The results presented in Table 6 show that pre-training-based strategies, including Transfer, TPP with DINO, and TPP with MAE, outperform the static random initialization strategy, Zero, demonstrating the advantage of pre-training. Notably, TPP with MAE achieved the best results on most metrics across all datasets, highlighting its superiority.

Target Parameter Pre-training on Another Data

In the target parameter pre-training stage, the pre-training data is directly from the target dataset. In this section, we explore the performance impact of using another dataset for pre-training in a cross-validation manner. Specifically, in our study, we adopted five datasets with three modalities for evaluation. Therefore, we adopted TPP on one dataset and fine-tuned the pre-trained model on all datasets. The results were shown in Table 7. We also recorded the performance of Adapter as the baseline. We observe that TPP obtains superior performance when pre-training data and fine-tuning data have identical modalities, especially having the same dataset, which usually results in the best performance. Moreover, using another modality data for pre-training even obtains negative effects, resulting in worse performance than Adapter. In summary, the TPP can only achieve its maximum effectiveness when pre-trained on data that is either the same as or in the same modalities as the target data.

Conclusions

In this paper, we propose an efficient fine-tuning framework for medical image analysis, termed Target Parameter Pre-training (TPP). Guided by the principle that *if the backbone is pre-trained, the newly added parameters should also be pre-trained*, we introduce a target parameter pre-training stage. This stage, implemented before fine-tuning, pre-trains the parameters introduced by PEFT methods that involve adding new parameters. Our TPP framework is versatile, allowing for the integration of various pretext tasks for pre-training and supporting different PEFT methods as backbones. We conducted experiments using two state-of-the-art generative and contrastive learning methods, MAE and DINO, for pre-training, and four advanced PEFT methods as backbones. The results showed consistent improvements across five datasets, validating the effectiveness of the

	Retinal OCT-C8			GlaS	
	Acc	AUC	F1	Dice	HD
Adapter	95.36	99.74	95.36	88.98	49.06
Adapter w/ TPP	96.25	99.75	96.24	88.60	46.98
VPT	89.32	99.04	89.25	86.27	52.23
VPT w/ TPP	91.14	99.24	91.13	87.06	58.63
SSF	88.68	98.93	88.66	87.64	54.49
SSF w/TPP	89.82	99.12	89.81	88.07	56.43

Table 1: Results on three PEFT Methods based on TPP. For TPP, we used DINO as the pretext task. We highlighted in **bold** the better results comparing each PEFT method with and without TPP.

proposed TPP framework. In future work, we plan to investigate the correlations between the pretext tasks used in backbone pre-training and those employed in target parameter pre-training.

Acknowledgments

This work was supported in part by the National Natural Science Foundation of China under Grants 62171377, in part by the Ningbo Clinical Research Center for Medical Imaging under Grant 2021L003 (Open Project 2022LYKFZD06), and in part by Shenzhen Science and Technology Program under Grants JCYJ20220530161616036.

Appendix

A. TPP based on DINO

In this paper, we conducted experiments on the MHIST and QaTa datasets using TPP based on DINO. To further validate our framework, we extended our evaluation to the Retinal OCT-C8 and GlaS datasets, as summarized in Table 1. The results indicate that incorporating TPP consistently enhances performance across most metrics. For instance, SSF with TPP demonstrates improvements of 1.14%, 0.19%, 1.15%, and 0.43% in Retinal OCT-C8’s ACC, AUC, F1, and GlaS’s Dice scores, respectively.

B. Ablation Experiments

Mask Ratio. We evaluated the impact of different mask ratios for the Adapter with TPP, based on MAE, across the Chest X-ray PD and QaTa datasets. The results are presented in Table 2 and Table 3. Our analysis reveals a discrepancy between the optimal mask ratios for classification and segmentation tasks. Specifically, the optimal mask ratio for classification tasks tends to be lower than for segmentation tasks. For example, the highest performance on the Chest X-ray PD dataset (a classification dataset) is achieved with a mask ratio of 0.75, whereas a mask ratio of 0.85 yields the best results on the QaTa dataset (a segmentation dataset). Table 5 details the settings for all five datasets, with mask ratios consistent with our findings.

Decoder update strategy for TPP based on MAE. In this study, we employed the ViT/B model pre-trained using the MAE framework as the backbone. Consequently, when

Mask Ratio	ACC	AUC	F1
0.65	95.71	99.21	95.70
0.70	95.49	99.19	95.46
0.75	95.93	99.21	95.91
0.80	95.49	99.14	95.46

Table 2: Results for TPP based on MAE with different mask ratios on the Chest X-ray PD dataset. The backbone is Adapter. The best result on each column is highlighted in **bold**.

Mask Ratio	Dice	HD
0.75	78.88	29.62
0.80	79.26	30.00
0.85	79.50	29.28
0.90	79.30	29.46

Table 3: Results for TPP based on MAE with different mask ratios on the QaTa dataset. The backbone is Adapter. The best result on each column is highlighted in **bold**.

	Chest X-ray PD			QaTa	
	ACC	AUC	F1	Dice	HD
Freeze	95.93	99.21	95.91	79.01	29.45
Update	94.94	99.32	94.90	79.50	29.28

Table 4: Results of freezing versus updating the decoder parameters using TPP, based on MAE, on the Chest X-ray PD and QaTa datasets. The best result on each column is highlighted in **bold**.

MAE is utilized as the pretext task for target parameter pre-training, the decoder also inherits pre-trained parameters. We loaded these pre-trained parameters and conducted experiments to assess the impact of updating versus freezing them. The results, presented in Table 4, indicate that freezing the pre-trained decoder positively influences classification tasks but has a detrimental effect on segmentation tasks. Based on these empirical findings, we opted to freeze the decoder parameters for classification tasks while allowing updates for segmentation tasks.

C. Implementation details

Image sizes of the datasets. The images in the MHIST and QaTa datasets were originally sized at 224×224 pixels. For the Retinal OCT-C8 dataset, image dimensions varied from 384×496 to 1536×496 pixels. All images were resized to 224×224 pixels for consistency. Similarly, the Chest X-ray PD dataset, with original image sizes ranging from 224×224 to 5623×4757 pixels, was uniformly resized to 224×224 pixels. The GlaS dataset, initially at 522×775 pixels, was resized to 512×512 pixels.

Details of the five downstream tasks. Table 6 provides the implementation details for five downstream datasets: MHIST, Retinal OCT-C8, Chest X-ray PD, GlaS, and QaTa. The table includes information on the loss function, patch size, optimizer, learning rate, batch size, and maximum iterations. Given the sensitivity of the PEFT methods to the

	MHIST	Retinal OCT-C8	Chest X-ray PD	GlaS	QaTa
Adapter w/ TPP	0.75	0.75	0.75	0.85	0.85
EVP w/TPP	0.75	0.75	0.75	0.80	0.90
VPT w/TPP	0.75	0.75	0.75	0.85	0.85
SSF w/TPP	0.75	0.75	0.75	0.85	0.85

Table 5: Mask ratio of PEFT methods with TPP based on MAE.

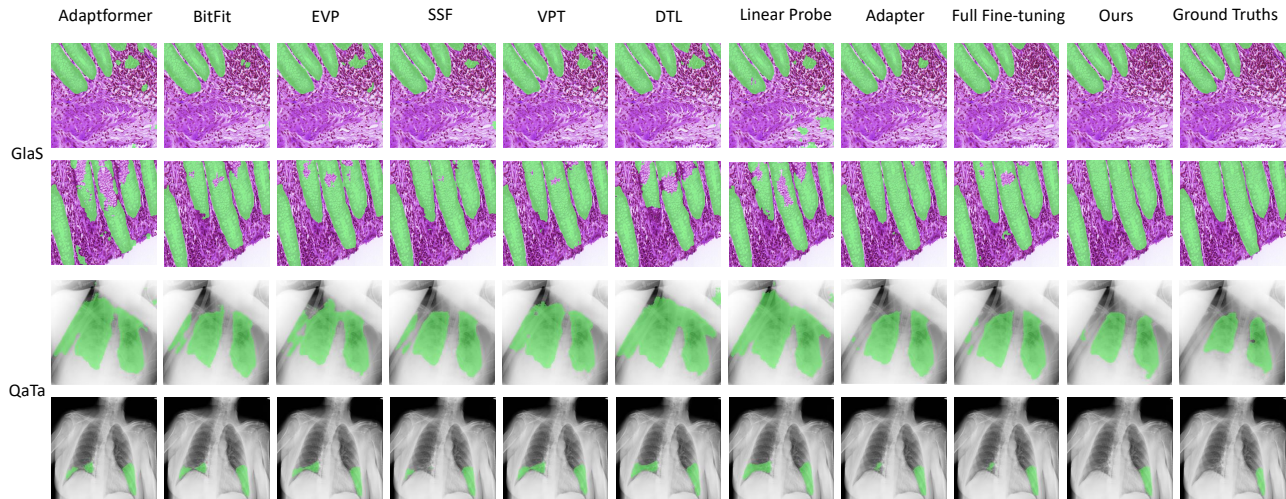


Figure 1: Visualization of segmentation results obtained by Adaptformer, BitFit, EVP, SSF, VPT, DTL, Linear Probe, Adapter, Full Fine-tuning, Ours, and Ground Truths. The pneumonia and malignant regions are colored green.

Dataset	Loss Function	Patch Size	Optimizer	Learning Rate	Batch Size	Iterations
MHIST	CE	224×224	AdamW	Grid Search	32	2,700
Retinal OCT-C8	CE	224×224	AdamW	0.0001	32	57,500
Chest X-ray PD	CE	224×224	AdamW	0.00005	32	1,980
GlaS	Dice+CE	512×512	AdamW	0.0001	4	25,000
QaTa	Dice+CE	224×224	AdamW	0.0001	16	25,000

Table 6: Implementation details of five downstream tasks. CE: cross-entropy loss function.

Method	Full Fine-tuning	Linear Probe	EVP	VPT	SSF	BitFit	Adapter	Adaptformer	DTL
Learning Rate	0.00001	0.01	0.00005	0.0001	0.001	0.001	0.0001	0.001	0.005

Table 7: Learning rate of PEFT methods on the MHIST dataset.

learning rate for the MHIST dataset, we conducted a grid search to determine the optimal value within the range of 0.000005 to 0.05. The learning rates that yield the best performance for each PEFT method are reported in Table 7.

D. Visualization of Segmentation Results

To facilitate a qualitative comparison, we visualized the segmentation results produced by Adaptformer, BitFit, EVP, SSf, VPT, Linear Probe, Adapter, Full Fine-tuning, and our proposed method, Adapter with TPP, across two datasets, as depicted in Figure 1. These visualizations demonstrate that the segmentation results from our approach more closely match the ground truth, effectively mitigating issues related to over-segmentation and under-segmentation. For instance,

in the second row of the figure, the segmentation of glandular tissue produced by all competing methods suffers from under-segmentation, whereas our TPP method achieves a more accurate segmentation. In particular, compared to Full Fine-tuning, our method achieves a comparable result in the first row and obtains more accurate segmentation results in the remaining rows.

References

- Akhoulfi, M. A.; and Chetoui, M. 2021. Chest XR COVID-19 detection. <https://cxr-covid19.grand-challenge.org/>. Online; accessed September 2021.
- Asraf, A.; and Islam, Z. 2021. COVID19, pneumonia and normal chest X-ray PA dataset. Mendeley Data V1 (2021).

- Awan, R.; Sirinukunwattana, K.; Epstein, D.; Jefferyes, S.; Qidwai, U.; Aftab, Z.; Mujeeb, I.; Snead, D.; and Rajpoot, N. 2017. Glandular morphometrics for objective grading of colorectal adenocarcinoma histology images. *Scientific reports*, 7(1): 16852.
- Azizi, S.; Mustafa, B.; Ryan, F.; Beaver, Z.; Freyberg, J.; Deaton, J.; Loh, A.; Karthikesalingam, A.; Kornblith, S.; Chen, T.; et al. 2021. Big self-supervised models advance medical image classification. In *Proceedings of the IEEE/CVF international conference on computer vision*, 3478–3488.
- Basu, S.; Hu, S.; Massiceti, D.; and Feizi, S. 2024. Strong Baselines for Parameter-Efficient Few-Shot Fine-Tuning. In *Proceedings of the AAAI Conference on Artificial Intelligence*, volume 38, 11024–11031.
- Caron, M.; Misra, I.; Mairal, J.; Goyal, P.; Bojanowski, P.; and Joulin, A. 2020. Unsupervised learning of visual features by contrasting cluster assignments. *Advances in neural information processing systems*, 33: 9912–9924.
- Caron, M.; Touvron, H.; Misra, I.; Jégou, H.; Mairal, J.; Bojanowski, P.; and Joulin, A. 2021. Emerging properties in self-supervised vision transformers. In *Proceedings of the IEEE/CVF international conference on computer vision*, 9650–9660.
- Chen, S.; Ge, C.; Tong, Z.; Wang, J.; Song, Y.; Wang, J.; and Luo, P. 2022. Adaptformer: Adapting vision transformers for scalable visual recognition. *Advances in Neural Information Processing Systems*, 35: 16664–16678.
- Chen, T.; Kornblith, S.; Norouzi, M.; and Hinton, G. 2020. A simple framework for contrastive learning of visual representations. In *International conference on machine learning*, 1597–1607. PMLR.
- Degerli, A.; Kiranyaz, S.; Chowdhury, M. E.; and Gabbouj, M. 2022. Osegnet: Operational segmentation network for covid-19 detection using chest x-ray images. In *2022 IEEE International Conference on Image Processing (ICIP)*, 2306–2310. IEEE.
- Devlin, J.; Chang, M.-W.; Lee, K.; and Toutanova, K. 2018. BERT: Pre-training of Deep Bidirectional Transformers for Language Understanding. *arXiv preprint arXiv:1810.04805*.
- Dosovitskiy, A.; Beyer, L.; Kolesnikov, A.; Weissenborn, D.; Zhai, X.; Unterthiner, T.; Dehghani, M.; Minderer, M.; Heigold, G.; Gelly, S.; et al. 2020. An image is worth 16x16 words: Transformers for image recognition at scale. *arXiv preprint arXiv:2010.11929*.
- Dutt, R.; Ericsson, L.; Sanchez, P.; Tsafaris, S. A.; and Hospedales, T. 2023a. Parameter-efficient fine-tuning for medical image analysis: The missed opportunity. *arXiv preprint arXiv:2305.08252*.
- Dutt, R.; Ericsson, L.; Sanchez, P.; Tsafaris, S. A.; and Hospedales, T. 2023b. Parameter-efficient fine-tuning for medical image analysis: The missed opportunity. *arXiv preprint arXiv:2305.08252*.
- Frankle, J.; Schwab, D. J.; and Morcos, A. S. 2020. Training batchnorm and only batchnorm: On the expressive power of random features in cnns. *arXiv preprint arXiv:2003.00152*.
- Fu, M.; Zhu, K.; and Wu, J. 2024. Dtl: Disentangled transfer learning for visual recognition. In *Proceedings of the AAAI Conference on Artificial Intelligence*, volume 38, 12082–12090.
- Gharawi, A.; Alahmadi, M. D.; and Ramaswamy, L. 2023. Self-Supervised Skin Lesion Segmentation: An Annotation-Free Approach. *Mathematics*, 11(18): 3805.
- Goodfellow, I.; Pouget-Abadie, J.; Mirza, M.; Xu, B.; Warde-Farley, D.; Ozair, S.; Courville, A.; and Bengio, Y. 2020. Generative adversarial networks. *Communications of the ACM*, 63(11): 139–144.
- He, A.; Wang, K.; Wang, Z.; Li, T.; and Fu, H. 2023. DVPT: Dynamic Visual Prompt Tuning of Large Pre-trained Models for Medical Image Analysis. *arXiv preprint arXiv:2307.09787*.
- He, K.; Chen, X.; Xie, S.; Li, Y.; Dollár, P.; and Girshick, R. 2022. Masked autoencoders are scalable vision learners. In *Proceedings of the IEEE/CVF conference on computer vision and pattern recognition*, 16000–16009.
- He, K.; Fan, H.; Wu, Y.; Xie, S.; and Girshick, R. 2020. Momentum contrast for unsupervised visual representation learning. In *Proceedings of the IEEE/CVF conference on computer vision and pattern recognition*, 9729–9738.
- Houlsby, N.; Giurgiu, A.; Jastrzebski, S.; Morrone, B.; De Laroussilhe, Q.; Gesmundo, A.; Attariyan, M.; and Gelly, S. 2019. Parameter-efficient transfer learning for NLP. In *International conference on machine learning*, 2790–2799. PMLR.
- Hu, E. J.; Shen, Y.; Wallis, P.; Allen-Zhu, Z.; Li, Y.; Wang, S.; Wang, L.; and Chen, W. 2021. Lora: Low-rank adaptation of large language models. *arXiv preprint arXiv:2106.09685*.
- Huang, Y.; Cheng, P.; Tam, R.; and Tang, X. 2024. FPT: Fine-grained Prompt Tuning for Parameter and Memory Efficient Fine Tuning in High-resolution Medical Image Classification. *arXiv preprint arXiv:2403.07576*.
- Jia, M.; Tang, L.; Chen, B.-C.; Cardie, C.; Belongie, S.; Hariharan, B.; and Lim, S.-N. 2022. Visual prompt tuning. In *European Conference on Computer Vision*, 709–727. Springer.
- Kather, J. N.; Halama, N.; and Marx, A. 2018. 100,000 histological images of human colorectal cancer and healthy tissue.
- Kermany, D.; Zhang, K.; Goldbaum, M.; et al. 2018. Labeled optical coherence tomography (oct) and chest x-ray images for classification. *Mendeley data*, 2(2): 651.
- Li, X. L.; and Liang, P. 2021. Prefix-tuning: Optimizing continuous prompts for generation. *arXiv preprint arXiv:2101.00190*.
- Lian, D.; Zhou, D.; Feng, J.; and Wang, X. 2022. Scaling & shifting your features: A new baseline for efficient model tuning. *Advances in Neural Information Processing Systems*, 35: 109–123.
- Liao, B.; Tan, S.; and Monz, C. 2024. Make pre-trained model reversible: From parameter to memory efficient fine-tuning. *Advances in Neural Information Processing Systems*, 36.

- Liu, W.; Shen, X.; Pun, C.-M.; and Cun, X. 2023. Explicit visual prompting for low-level structure segmentations. In *Proceedings of the IEEE/CVF Conference on Computer Vision and Pattern Recognition*, 19434–19445.
- Loshchilov, I.; Hutter, F.; et al. 2017. Fixing weight decay regularization in adam. *arXiv preprint arXiv:1711.05101*, 5.
- Michelucci, U. 2022. An introduction to autoencoders. *arXiv preprint arXiv:2201.03898*.
- Ronneberger, O.; Fischer, P.; and Brox, T. 2015. U-net: Convolutional networks for biomedical image segmentation. In *Medical image computing and computer-assisted intervention—MICCAI 2015: 18th international conference, Munich, Germany, October 5-9, 2015, proceedings, part III 18*, 234–241. Springer.
- Siméoni, O.; Puy, G.; Vo, H. V.; Roburin, S.; Gidaris, S.; Bursuc, A.; Pérez, P.; Marlet, R.; and Ponce, J. 2021. Localizing objects with self-supervised transformers and no labels. *arXiv preprint arXiv:2109.14279*.
- Sirinukunwattana, K.; Pluim, J. P.; Chen, H.; Qi, X.; Heng, P.-A.; Guo, Y. B.; Wang, L. Y.; Matuszewski, B. J.; Bruni, E.; Sanchez, U.; et al. 2017. Gland segmentation in colon histology images: The glas challenge contest. *Medical image analysis*, 35: 489–502.
- Song, Z.; Yang, K.; Guan, N.; Zhu, J.; Qiao, P.; and Hu, Q. 2023. Pvp: Pre-trained visual parameter-efficient tuning. *arXiv preprint arXiv:2304.13639*.
- Su, Y.; Wang, X.; Qin, Y.; Chan, C.-M.; Lin, Y.; Wang, H.; Wen, K.; Liu, Z.; Li, P.; Li, J.; et al. 2021. On transferability of prompt tuning for natural language processing. *arXiv preprint arXiv:2111.06719*.
- Subramanian, M.; Shanmugavadivel, K.; Naren, O. S.; Premkumar, K.; and Rankish, K. 2022. Classification of retinal oct images using deep learning. In *2022 international conference on computer communication and informatics (ICCCI)*, 1–7. IEEE.
- Sung, Y.-L.; Cho, J.; and Bansal, M. 2022. Lst: Ladder side-tuning for parameter and memory efficient transfer learning. *Advances in Neural Information Processing Systems*, 35: 12991–13005.
- Tang, N.; Fu, M.; Zhu, K.; and Wu, J. 2024. Low-rank Attention Side-Tuning for Parameter-Efficient Fine-Tuning. *arXiv preprint arXiv:2402.04009*.
- Touvron, H.; Cord, M.; El-Nouby, A.; Verbeek, J.; and Jégou, H. 2022. Three things everyone should know about vision transformers. In *European Conference on Computer Vision*, 497–515. Springer.
- Vincent, P.; Larochelle, H.; Bengio, Y.; and Manzagol, P.-A. 2008. Extracting and composing robust features with denoising autoencoders. In *Proceedings of the 25th international conference on Machine learning*, 1096–1103.
- Wang, Y.; Cheng, L.; Fang, C.; Zhang, D.; Duan, M.; and Wang, M. 2024. Revisiting the power of prompt for visual tuning. *arXiv preprint arXiv:2402.02382*.
- Wei, J.; Suriawinata, A.; Ren, B.; Liu, X.; Lisovsky, M.; Vaickus, L.; Brown, C.; Baker, M.; Tomita, N.; Torresani, L.; et al. 2021. A petri dish for histopathology image analysis. In *Artificial Intelligence in Medicine: 19th International Conference on Artificial Intelligence in Medicine, AIME 2021, Virtual Event, June 15–18, 2021, Proceedings*, 11–24. Springer.
- Willeminck, M. J.; Koszek, W. A.; Hardell, C.; Wu, J.; Fleischmann, D.; Harvey, H.; Folio, L. R.; Summers, R. M.; Rubin, D. L.; and Lungren, M. P. 2020. Preparing medical imaging data for machine learning. *Radiology*, 295(1): 4–15.
- Yang, C.; Wu, Z.; Zhou, B.; and Lin, S. 2021. Instance localization for self-supervised detection pretraining. In *Proceedings of the IEEE/CVF Conference on Computer Vision and Pattern Recognition*, 3987–3996.
- Ye, Y.; Xie, Y.; Zhang, J.; Chen, Z.; Wu, Q.; and Xia, Y. 2024. Continual self-supervised learning: Towards universal multi-modal medical data representation learning. In *Proceedings of the IEEE/CVF Conference on Computer Vision and Pattern Recognition*, 11114–11124.
- Ye, Y.; Zhang, J.; Chen, Z.; and Xia, Y. 2022. Desd: Self-supervised learning with deep self-distillation for 3d medical image segmentation. In *International Conference on Medical Image Computing and Computer-Assisted Intervention*, 545–555. Springer.
- Yin, D.; Han, X.; Li, B.; Feng, H.; and Bai, J. 2023. Parameter-efficient is not sufficient: Exploring parameter, memory, and time efficient adapter tuning for dense predictions. *arXiv preprint arXiv:2306.09729*.
- Yoo, S.; Kim, E.; Jung, D.; Lee, J.; and Yoon, S. 2023. Improving visual prompt tuning for self-supervised vision transformers. In *International Conference on Machine Learning*, 40075–40092. PMLR.
- Zaken, E. B.; Ravfogel, S.; and Goldberg, Y. 2021. Bitfit: Simple parameter-efficient fine-tuning for transformer-based masked language-models. *arXiv preprint arXiv:2106.10199*.
- Zhang, Q.; Chen, M.; Bukharin, A.; Karampatziakis, N.; He, P.; Cheng, Y.; Chen, W.; and Zhao, T. 2023. AdaLoRA: Adaptive budget allocation for parameter-efficient fine-tuning. *arXiv preprint arXiv:2303.10512*.
- Zhong, Z.; Tang, Z.; He, T.; Fang, H.; and Yuan, C. 2024. Convolution meets lora: Parameter efficient finetuning for segment anything model. *arXiv preprint arXiv:2401.17868*.
- Zhou, H.-Y.; Lu, C.; Yang, S.; Han, X.; and Yu, Y. 2021. Preservation learning improves self-supervised medical image models by reconstructing diverse contexts. In *Proceedings of the IEEE/CVF International Conference on Computer Vision*, 3499–3509.
- Zhou, Z.; Siddiquee, M. M. R.; Tajbakhsh, N.; and Liang, J. 2019. Unet++: Redesigning skip connections to exploit multiscale features in image segmentation. *IEEE transactions on medical imaging*, 39(6): 1856–1867.